symmetry coordinates are listed in Table V. Our LDF force field for H_2NCN is in good general agreement with that previously published[24] by Ichikawa et al. at the 4-31G* level of theory, if it is kept in mind that the frequencies at the 4-31G* level are on average about 10% higher than the experimental ones. The potential energy distributions are given in Table V and support the given mode descriptions.

A special comment is required on the magnitudes of F_{99} in our force fields, which are given in Table VI. The listed F_{99} values are clearly too high and should be comparable to those of F_{55}. The $\nu_5(A')$ and $\nu_9(A'')$ modes represent the in-plane and out-of-plane deformations of the nearly linear NXN groups, which, therefore, should be almost degenerate and exhibit similar frequencies and force constants. Whereas the frequencies of ν_9 are comparable to those of ν_5, the F_{99} values in Table VI are about 2-4 times larger than those of F_{55}. This is an artifact caused by the inability to exactly describe with our computer input code the S_9 symmetry coordinate of the out-of-plane NXN deformation for these molecules when they possess a slightly bent NXN group. Our program to convert the Cartesian second derivatives to symmetry-adapted internal coordinates allows for only four kinds of internal motions: bond stretching, angle bending, a dihedral angle between two planes, and the minimum angle that a bond forms with a plane. Thus, the $\nu_9(A'')$ mode had to be defined as the sum of the angles formed between the X-N(2) bond and the two planes defined by H(1)N(1)X and H(2)N(1)X. By making the NXN bonds linear, we were able to properly describe S_9 with this code and obtain values for F_{99} ($H_2N_3^+$, 0.47 mdyn/Å; H_2N-CN, 0.44 mdyn/Å) that are in excellent agreement with our expectations (see above) and those previously reported.[24] The PED ($94S_9 + 6S_8$) for the revised F_{99} values was similar to those given in Table V, while the remainder of the A'' force field remained practically unchanged.

Acknowledgment. The authors thank Dr. C. J. Schack and Mr. R. D. Wilson for their help, Dr. R. Minkwitz for bringing his unpublished studies on $H_2N_3^+SbCl_6^-$ to our attention, and the U.S. Army Research Office and the U.S. Air Force Phillips Laboratory for financial support of the work at Rocketdyne. T.M. thanks the Deutsche Forschungs Gemeinschaft for the provision of a postdoctoral fellowship.

Supplementary Material Available: Table 1S, listing anisotropic temperature factors (1 page); Table 2S, listing observed and calculated structure factors (3 pages). Ordering information is given on any current masthead page.

The Vanadium(IV) Enterobactin Complex: Structural, Spectroscopic, and Electrochemical Characterization[1]

Timothy B. Karpishin, Torin M. Dewey, and Kenneth N. Raymond*

Contribution from the Department of Chemistry, University of California, Berkeley, California 94720. *Received August 24, 1992*

Abstract: The siderophore enterobactin (H_6ent) has been crystallized as the vanadium(IV) complex in the compound K_2[V(ent)]·3DMF from dimethylformamide (DMF) solution. The pseudooctahedral coordination of the metal ion is through the three catechol groups and has approximate C_3 molecular point symmetry. The geometry is intermediate between trigonal prismatic and octahedral, with a twist angle of 28°. For comparison, the unconstrained complex of *N*-ethyl-2,3-dihydroxybenzamide (H_2eba) has been determined. The twist angle in $[V(eba)_3]^{2-}$ is 36°, somewhat larger than in the constrained enterobactin complex. The other metrical parameters are essentially identical between the two. Both the stability and the Δ chirality of the enterobactin complex are explained as due to the conformation of the triserine backbone. Molecular modeling calculations correctly predict this chiral preference as well as that for the complex of the (linear trimer) enterobactin hydrolysis product. The V-O bond distances in $[V(ent)]^{2-}$ average 1.946(7) and 1.939(5) Å to the ortho and meta catechol oxygens, respectively. Hydrogen bonding between the amide proton and the ortho catechol oxygen is an important feature of the structure. Comparison of the conformation of the trilactone serine ring in the vanadium enterobactin complex with two related trilactones shows that the conformation seen is characteristic of this triserine structure and is not a result of the metal complexation or of hydrogen bonding within the triserine ring. This also implies that the free ligand has a conformation similar to that seen in the metal complex. The potassium cations are partially coordinated by the meta catechol oxygens. Molecular modeling indicates that a smaller cation such as calcium cannot fit in the cavity formed between the octahedral catechol coordination site and the triserine ring. The UV/vis spectrum of $[V(ent)]^{2-}$ has been assigned on the basis of earlier quantitative spectroscopic studies. The spectroscopic parameters indicate that the M-O bonding is stronger in the vanadium complex than in the iron complex of enterobactin, partially due to strong π bonding. A quasi reversible reduction potential (in DMF vs SCE) is found for the V^V/V^{IV} couple of +0.39 V. For K_2[V(ent)]·3DMF, space group $P2_1$, a = 13.164(3), b = 10.001(1), c = 16.600(2) Å, β = 93.96°, z = 2, V = 2180(1) Å^3. For 5551 unique data with $F_o^2 > 3\sigma(F_o^2)$ R = 0.049, R_w = 0.062. For K_2[V(eba)$_3$]·3DMF, space group $Pa\bar{3}$, a = 20.632(5) Å, z = 8, V = 8783(5) Å^3. For 2526 unique data with $F_o^2 > 3\sigma(F_o^2)$ R = 0.051, R_w = 0.058.

Introduction

Most aerobic and anaerobic bacteria synthesize and excrete low molecular weight compounds (siderophores) for the solubilization and transport of iron.[2-4] Since the iron supply is often a limiting factor in the growth of these microbes, siderophores and their corresponding transport systems play an important role in bacterial virulence.[5] Of the approximately 200 siderophores now discovered, enterobactin (Figure 1), produced by enteric bacteria such as *Escherichia coli*, has received considerable attention. Since its discovery in 1970,[6,7] the synthesis,[8-10] biosynthesis,[11] microbial transport,[5,12-14] and solution thermodynamics[15-17]

* To whom correspondence should be addressed.

(1) Paper number 49 in the series Coordination Chemistry of Microbial Iron Transport. The previous paper (number 48) in this series: Abu-Dari, K.; Raymond, K. N. *J. Coord. Chem.* **1992**, *26*, 1-14. [Note that the series number cited in that article is incorrect. Papers 47 and 46 in the series are ref 31 and 28 of this paper, respectively.]

(2) Matzanke, B. F.; Müller-Matzanke, G.; Raymond, K. N. In *Iron Carriers and Iron* Proteins; Loehr, T. M., Ed.; VCH Publishers: New York, 1989; p. 1.

(3) Raymond, K. N.; Müller, G.; Matzanke, B. F. *Top. Curr. Chem.* **1984**, *123*, 49.

0002-7863/93/1515-1842$04.00/0

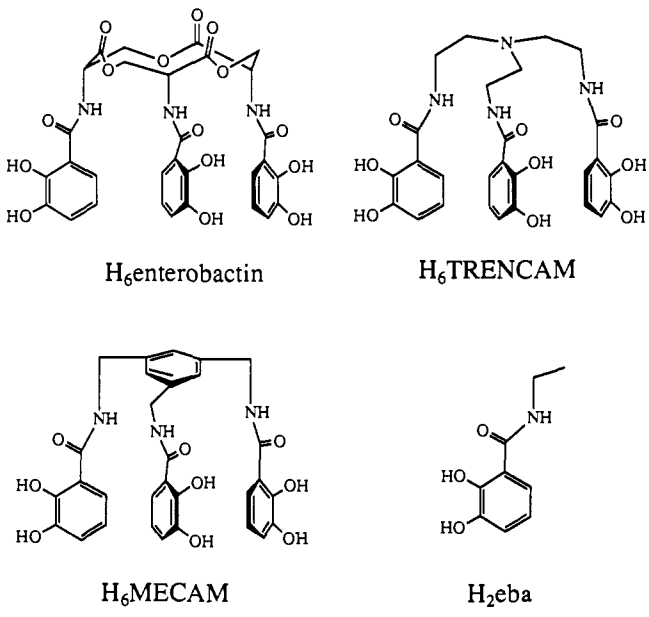

Figure 1. Structures of the ligands discussed in this study.

of enterobactin have been investigated. The thermodynamic studies have shown that enterobactin forms the most stable Fe^{III} complex known, with a formal stability constant of 10^{49}.[16] The enterobactin molecule is 3-fold symmetric and is comprised of three catecholate groups suspended from a trilactone backbone (Figure 1); metal coordination at neutral pH occurs through the six catecholate oxygens.

Because of its remarkable sequestering properties, enterobactin has been a model for the development of synthetic chelators—particularly for clinical use in the treatment of iron overload or iron poisoning.[18] Although several tris(catecholate) chelators have been prepared in this laboratory, the synthetic molecules consistently have lower formation constants and binding efficiencies at pH 7.4 than enterobactin. Hence, one particular goal has been the explanation of the extraordinarily high stability of ferric enterobactin, $[Fe(ent)]^{3-}$, compared to model compounds such as $[Fe(TRENCAM)]^{3-}$ [19] and $[Fe(MECAM)]^{3-}$ (Figure 1).[18,20-22] The difference in the aqueous stability between $[Fe(ent)]^{3-}$ and these compounds is on the order of 10^6.[16] Although the high stability of iron(III) tris(catecholate) complexes has been addressed in a general fashion from the spectroscopy and bonding,[23] the source of the smaller stability differences *among* tris(catecholate) complexes cannot be so identified. Details of the three-dimensional structures of these complexes can potentially provide this information. Since an X-ray crystal structure of $[Fe(ent)]^{3-}$, or any enterobactin–metal complex, has so far been elusive, previous investigations regarding structure have included a conformational analysis from NMR spectra of the diamagnetic Ga^{III} complex[24] and molecular mechanics calculations of the Fe^{III} complex.[25] Although Ga^{III} and Fe^{III} tris(catecholate) complexes are typically isostructural,[26-28] these two analyses differ substantially in specific aspects of the predicted structures of $[Ga(ent)]^{3-}$ and $[Fe(ent)]^{3-}$.

Other studies regarding structure have probed the trischelate chirality of enterobactin–metal complexes. Since the backbone of enterobactin is derived from three *l*-serine units, the Δ and Λ isomers are diastereomeric. The Fe^{III}, Cr^{III}, and Rh^{III} enterobactin complexes all have been shown, from circular dichroism spectra, to be preferentially Δ (a right handed propeller).[28-30] This is in contrast to siderophores such as ferrichrome that stereospecifically complex metal ions in a Λ conformation.[2] Although several laboratories over two decades have attempted to crystallize $[Fe(ent)]^{3-}$, no crystal structure analysis has been available for any enterobactin complex. Recently crystals of the vanadium(IV) complex were obtained, and we have previously communicated details of the single-crystal X-ray structure of $[V(ent)]^{2-}$.[31] In this paper, a full description of the three-dimensional structure of $[V(ent)]^{2-}$ is reported in addition to further characterization and structural comparisons.

The complex anion, $[V(ent)]^{2-}$, can be thought of as being comprised of four distinct moieties: the three catecholamide binding subunits and the 12-membered ring backbone. As part of a full analysis of the structure, the binding subunits in $[V(ent)]^{2-}$ are compared to the structure of the tris(bidentate) complex $[V(eba)_3]^{2-}$ (Figure 1) which we have determined and report here. Secondly, the backbone of $[V(ent)]^{2-}$ is compared to the structure of the cyclic trilactone which has been reported.[32] Together these comparisons explicate the structure of $[V(ent)]^{2-}$. Because of the similarities in the structures of V^{IV} and Fe^{III} complexes, the major features seen in $[V(ent)]^{2-}$ must also apply to $[Fe(ent)]^{3-}$, allowing the high stability of the native ferric complex to be addressed on the basis of its three-dimensional structure. The structure of $[V(ent)]^{2-}$ also permits an analysis of the interactions responsible for the stereoselective Δ-chelation observed in enterobactin–metal complexes.

Results and Discussion

The Structure of $[V(enterobactin)]^{2-}$. The complex anion is shown in stereo in Figure 2. The molecule is a trischelate through the three catecholate groups and has approximate C_3 molecular point symmetry. From this crystal structure the chirality at the vanadium center can be unequivocally assigned (see Experimental Section), and as can be seen from a view down the approximate

(4) In *Iron Transport in Microbes, Plants and Animals*; Winkelman, G., van der Helm, D., Neilands, J. B., Eds.; VCH Publishers: New York, 1987.
(5) Otto, B. R.; Verweij-van Vught, A. M. J. J.; MacLaren, D. M. *Critical Revs. Microbiol.* **1992**, *18*, 217-233.
(6) O'Brien, I. G.; Gibson, F. *Biochem. Biophys. Acta* **1970**, *215*, 393.
(7) Pollack, J. R.; Neilands, J. B. *Biochem. Biophys. Res. Commun.* **1970**, *38*, 989.
(8) Corey, E. J.; Bhattacharyya, S. *Tetrahedron Lett.* **1977**, 3919.
(9) Rastetter, W. H.; Erickson, T. J.; Venuti, M. C. *J. Org. Chem.* **1981**, *46*, 3579.
(10) Shanzer, A.; Libman, J. *J. Chem. Soc., Chem. Commun.* **1983**, 846.
(11) Rusnak, F.; Sakaitani, M.; Drueckhammer, D.; Reichert, J.; Walsh, C. T. *Biochemistry* **1991**, *30*, 2916.
(12) Ecker, D. J.; Matzanke, B. F.; Raymond, K. N. *J. Bacteriol.* **1986**, *167*, 666.
(13) Ecker, D. J.; Loomis, L. D.; Cass, M. E.; Raymond, K. N. *J. Am. Chem. Soc.* **1988**, *110*, 2457.
(14) Lodge, J. S.; Emery, T. *J. Bacteriol.* **1984**, *160*, 801.
(15) Scarrow, R. C.; Ecker, D. J.; Ng, C.; Liu, S.; Raymond, K. N. *Inorg. Chem.* **1991**, *30*, 900.
(16) Loomis, L. D.; Raymond, K. N. *Inorg. Chem.* **1991**, *30*, 906.
(17) Harris, W. R.; Carrano, C. J.; Cooper, S. R.; Sofen, S. R.; Avdeef, A. E.; McArdle, J. V.; Raymond, K. N. *J. Am. Chem. Soc.* **1979**, *101*, 6097.
(18) Harris, W. R.; Raymond, K. N. *J. Am. Chem. Soc.* **1979**, *101*, 6534.
(19) Rodgers, S. J.; Lee, C.-W.; Ng, C. Y.; Raymond, K. N. *Inorg. Chem.* **1987**, *26*, 1622.
(20) Venuti, M. C.; Rastetter, W. H.; Neilands, J. B. *J. Med. Chem.* **1979**, *22*, 123.
(21) Schuda, P. F.; Botti, C. M.; Venuti, M. C. *OPPI Briefs* **1984**, *16*, 119.
(22) Mitchell, M. S.; Walker, D.-L.; Whelan, J.; Bosnich, B. *Inorg. Chem.* **1987**, *26*, 396.
(23) Karpishin, T. B.; Gebhard, M. S.; Solomon, E. I.; Raymond, K. N. *J. Am. Chem. Soc.* **1991**, *113*, 2977.
(24) Llinās, M.; Wilson, D. M.; Neilands, J. B. *Biochemistry* **1973**, *12*, 3836.
(25) Shanzer, A.; Libman, J.; Lifson, S.; Felder, C. E. *J. Am. Chem. Soc.* **1986**, *108*, 7609.
(26) Raymond, K. N.; Isied, S. S.; Brown, L. D.; Fronczek, F. R.; Nibert, J. H. *J. Am. Chem. Soc.* **1976**, *98*, 1767.
(27) Borgias, B. A.; Barclay, S. J.; Raymond, K. N. *J. Coord. Chem.* **1986**, *15*, 109.
(28) Stack, T. D. P.; Karpishin, T. B.; Raymond, K. N. *J. Am. Chem. Soc.* **1992**, *114*, 1512.
(29) Isied, S. S.; Kuo, G.; Raymond, K. N. *J. Am. Chem. Soc.* **1976**, *98*, 1763.
(30) McArdle, J. V.; Sofen, S. R.; Cooper, S. R.; Raymond, K. N. *Inorg. Chem.* **1978**, *17*, 3075.
(31) Karpishin, T. B.; Raymond, K. N. *Angew. Chem., Int. Ed. Engl.* **1992**, *31*, 466.
(32) Shanzer, A.; Libman, J.; Frolow, F. *J. Am. Chem. Soc.* **1981**, *103*, 7339.

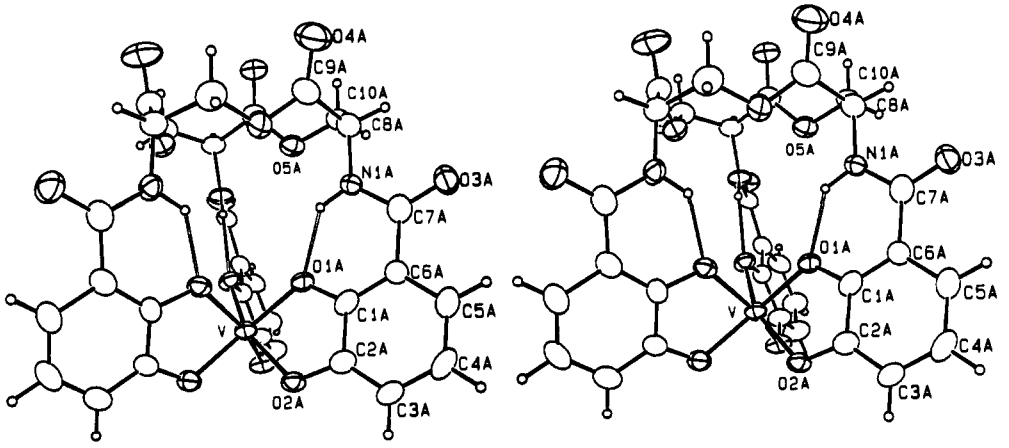

Figure 2. ORTEP stereoview of $[V(ent)]^{2-}$ with the molecular 3-fold axis vertical. The numbering scheme is shown for $^1/_3$ of the molecule. Fragments B (left in the figure) and C are similarly numbered.

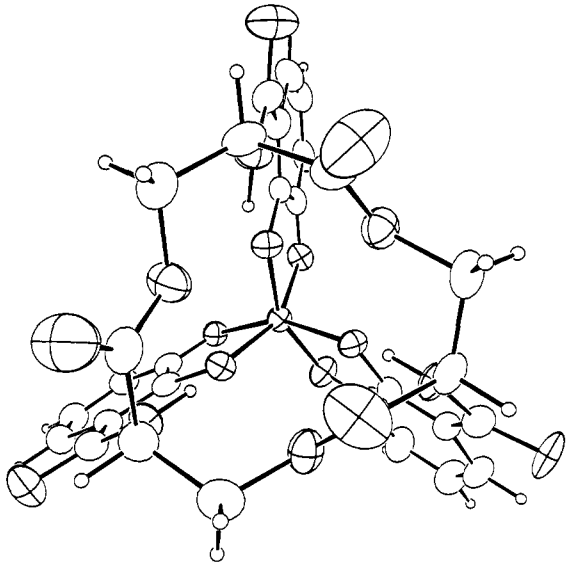

Figure 3. ORTEP diagram of $[V(ent)]^{2-}$ viewed down the approximate 3-fold axis.

molecular 3-fold axis (Figure 3), the chirality in $[V(ent)]^{2-}$ is Δ. The source of this stereospecific chelation can be ascribed to constraints within the backbone of enterobactin (vide infra).

From Figure 3 it is also evident that the complex is twisted considerably from octahedral geometry. The twist angle (0° for trigonal prismatic; 60° for octahedral)[33] in $[V(ent)]^{2-}$ is only 28°. By comparison, the twist angle in $[V(eba)_3]^{2-}$ is 36°. An ORTEP stereoview of $[V(eba)_3]^{2-}$ is shown in Figure 4. Repulsion energy calculations can be used to predict the optimum twist angle in a trischelate metal complex from the normalized bite of the bidentate ligands.[34] For $[V(ent)]^{2-}$ and $[V(eba)_3]^{2-}$, whose normalized bites are 1.283 and 1.287, respectively (see Table I), the calculated optimum twist angle for both complexes is 47°. Therefore, in $[V(eba)_3]^{2-}$, the observed twist angle is substantially lower (11°) than what the simple repulsion model would predict; this may be a result of π bonding.[35] The 8° lesser twist in $[V(ent)]^{2-}$ relative to $[V(eba)_3]^{2-}$, however, is likely a result of the cyclic backbone constraints. Since the catecholamide arms remain effectively planar to maximize the amide hydrogen bonding (vide infra), the twist angle at the metal center is a direct result of the effective twist of the C8–N1 bonds (see Figure 2). Since the C8 atoms are part of the cyclic enterobactin backbone, the angle at which the nitrogen atoms are suspended from the backbone is dependent upon the bonds within the backbone.

In a previous molecular mechanics calculation on $[Fe(ent)]^{3-}$, the authors assumed ideal octahedral geometry (twist angle 60°) around the iron center.[25] Since the twist angles in Fe^{III} tris(catecholate) complexes have been shown previously to be 4–6° larger than in V^{IV} complexes with the same ligands,[26,36–38] the twist angle in $[Fe(ent)]^{3-}$ is likely to be ≈33°. More accurate modeling of the structure of $[Fe(ent)]^{3-}$ would require incorporation of the appropriate geometry at the metal center (see below).

Although the metal ion is slightly smaller (V^{IV} = 0.58 Å; Fe^{III} = 0.65 Å),[39] the major features seen in the structure of $[V(ent)]^{2-}$ also apply to the $[Fe(ent)]^{3-}$ complex. Each of the complexes $[Fe(catecholate)_3]^{3-}$, $[V(catecholate)_3]^{2-}$, $[Fe(eba)_3]^{3-}$, and $[V(eba)_3]^{2-}$, has been structurally characterized,[26,36,40] and there are only slight differences between the V^{IV} and Fe^{III} complexes: V–O is typically 0.07 Å shorter than Fe–O and the V^{IV} twist angles are slightly smaller, as mentioned above. From analysis of the structure of $[V(ent)]^{2-}$, we conclude that a significant contributor to the stability of $[Fe(ent)]^{3-}$ is the optimum *size* of the enterobactin backbone. From the view in Figure 2, the 12-membered ring backbone appears ideally suited as a base from which the three catecholamide binding groups are suspended. The average V–O1 bond length (1.946(7) Å) is essentially the same as the average V–O2 bond length (1.939(5) Å), indicating that the binding subunits are perfectly positioned for coordination to a metal. In contrast, in the V^{III}[41] and Fe^{III}[28] structures of TRENCAM (whose Fe^{III} complex has an overall stability constant of $10^{43.6}$),[19] the two M–O bond lengths differ substantially. The M–O1 bond lengths are shorter by 0.022 (V^{III}) and 0.038 Å (Fe^{III}) than the M–O2 bond lengths in those structures. These results indicate that the TREN cap is too small to allow the catecholate groups to span effectively the coordination sphere. This argument, however, ignores the possible effect on the M–O2 bond lengths due to secondary potassium coordination. Since the potassium coordination can vary between structures,[42] a metrical parameter is needed which can be reliably used to discuss the orientation of the binding groups in these complexes. The distance from the metal to the carbon adjacent to the bound oxygen (i.e., M–C1 and M–C2, see Figure 2) is a parameter that better reflects the

(33) The twist angle is defined in trischelate metal complexes as the angle between two coordinating atoms of the same ligand projected onto the plane perpendicular to the idealized 3-fold axis.

(34) Kepert, D. L. In *Inorganic Stereochemistry*; Springer-Verlag: Berlin, 1982; p 92.

(35) We have recently shown that with certain metal ions (Ti^{IV}, V^{IV}, and Fe^{III}) within ligand constraints, π bonding in tris(catecholate) complexes can stabilize metal geometries close to trigonal prismatic: Karpishin, T. B.; Stack, T. D. P.; Raymond, K. N. *J. Am. Chem. Soc.* in press.

(36) Cooper, S. R.; Koh, Y. B.; Raymond, K. N. *J. Am. Chem. Soc.* **1982**, *104*, 5092.

(37) Dewey, T. M.; Raymond, K. N. Manuscript in preparation.

(38) Karpishin, T. B. Ph. D. Dissertation, University of California, Berkeley, 1992.

(39) Shannon, R. D. *Acta. Crystallogr., Sect. A* **1976**, *A32*, 751.

(40) Stack, T. D. P.; Raymond, K. N. Manuscript in preparation.

(41) Bulls, A. R.; Pippin, C. G.; Hahn, F. E.; Raymond, K. N. *J. Am. Chem. Soc.* **1990**, *112*, 2627.

(42) See the last paragraph of the paper regarding supplementary material.

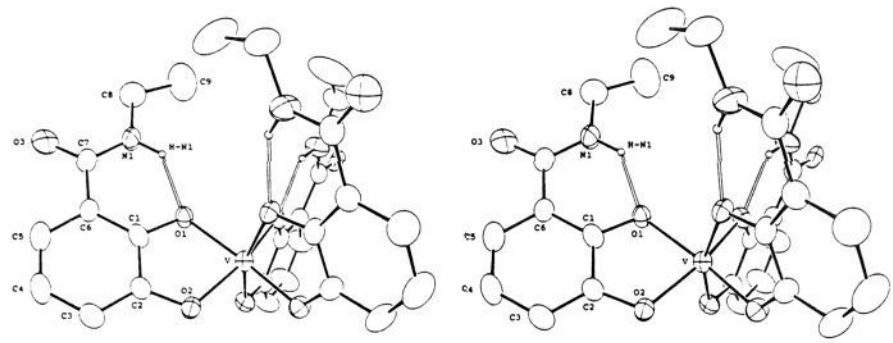

Figure 4. ORTEP stereoview of $[V(eba)_3]^{2-}$ with the molecular 3-fold axis vertical.

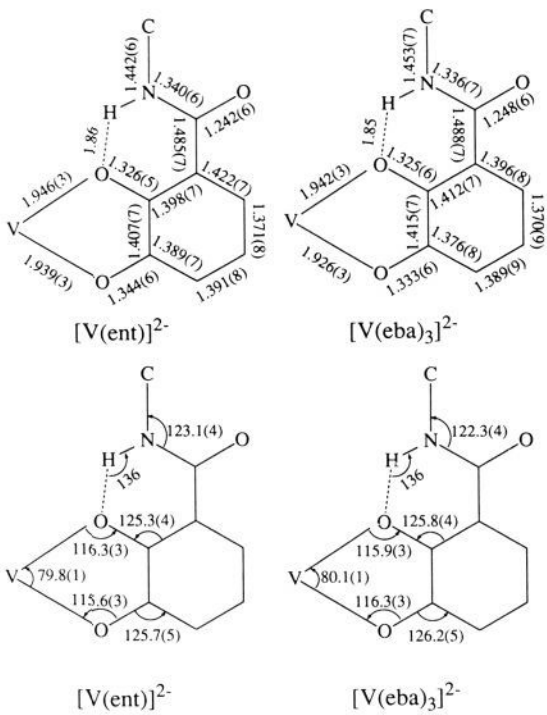

Figure 5. Comparison of the binding subunits of $[V(ent)]^{2-}$ and $[V(eba)_3]^{2-}$: top, bond lengths in Å; bottom, bond angles in degs.

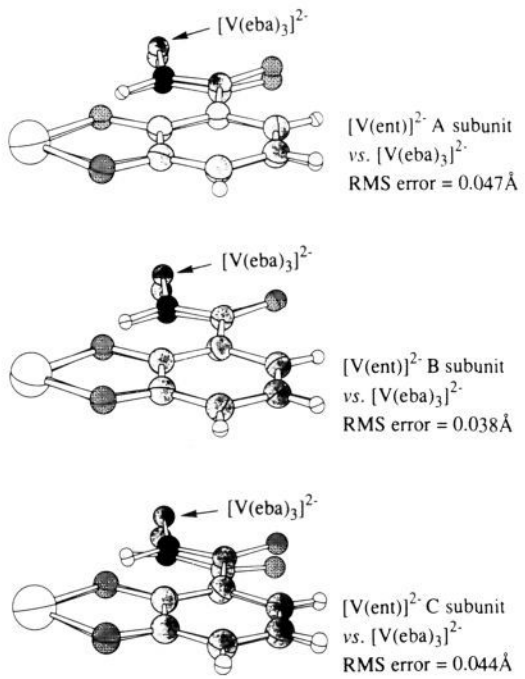

Figure 6. Overlay of the binding subunits of $[V(ent)]^{2-}$ with $[V(eba)_3]^{2-}$.

relative orientation of the catecholamide groups since it is not affected by potassium coordination. In $[V(ent)]^{2-}$, the average V–C1 distance is 2.797(5) Å and the average V–C2 distance is 2.796(5) Å. In $[V(TRENCAM)]^{3-}$ the V–C1 distance is 0.015 Å shorter than the V–C2 distance, and in $[Fe(TRENCAM)]^{3-}$, the Fe–C1 distance is 0.017 Å shorter than the Fe–C2 distance. These parameters therefore also reflect that in TRENCAM (and probably MECAM), the cap is too small for optimum binding of the subunits to the metal center. We thus conclude that the size of the enterobactin backbone plays a significant role in the high stability of the ferric complex.

A very important stabilizing feature in previously characterized tris(catecholamide) metal complexes,[41,43] and indeed in $[V(ent)]^{2-}$, is the hydrogen bonding between the amide protons and the catechol O1 oxygens (Figure 2). These three H-bonds form stable six-membered rings and result in planar catecholamide arms. The average NH—O distance is 1.86 Å in $[V(ent)]^{2-}$.[44] Although the earlier NMR study concluded that such H-bonding is not significant in $[Ga(ent)]^{3-}$,[24] the structures of $[V(ent)]^{2-}$ and the model compounds instead indicate that such hydrogen bonding is a key feature of the metal–enterobactin complex.

(43) McMurry, T. J.; Hosseini, M. W.; Garrett, T. M.; Hahn, F. E.; Reyes, Z. E.; Raymond, K. N. *J. Am. Chem. Soc.* **1987**, *109*, 7196.

(44) The amide hydrogens were placed 1.009 Å from the nitrogen atoms: Allen, F. H.; Kennard, O.; Watson, D. G.; Brammer, L.; Orpen, A. G.; Taylor, R. *J. Chem. Soc., Perkin Trans. II* **1987**, S1.

Table I. Structural Parameters for $[V(ent)]^{2-}$ and $[V(eba)_3]^{2-}$

	twist angle[a]	normalized bite[b]	NCO vs C_6 plane[c]
$[V(ent)]^{2-}$ A subunit	*28.2*	*1.289*	7.2
$[V(ent)]^{2-}$ B subunit	30.0	1.275	12.6
$[V(ent)]^{2-}$ C subunit	27.2	1.286	7.2
$[V(eba)_3]^{2-}$	36.3	1.287	4.9

[a] Reference 33. [b] Calculated from bite angle, θ(O–V–O); = 2 sin-(θ/2).[34] [c] Dihedral angle between amide plane (N1/C7/O3) and catechol (C1–C6) plane.

Comparison of $[V(ent)]^{2-}$ with $[V(eba)_3]^{2-}$. A further indication that the size of the enterobactin backbone is ideal for the three catecholamide groups to bind the metal is given by a comparison of the binding subunits of $[V(ent)]^{2-}$ and $[V(eba)_3]^{2-}$. Averaged bond lengths and angles of the two vanadium(IV) complexes are provided in Figure 5; there are no large distortions in the catecholamide groups of $[V(ent)]^{2-}$ relative to the coordination in the unconstrained trisbidentate complex. The single significant difference in the bond lengths and angles is the V–O2 length (1.939(3) Å in $[V(ent)]^{2-}$, 1.926(3) Å in $[V(eba)_3]^{2-}$). This is likely a result of differences in the potassium coordination to O2 in the solid state (vide supra). In both structures, the V–C1 distances are equivalent to the V–C2 distances: $[V(ent)]^{2-}$, $\Delta(V-C_{1,2}) = 0.002$ Å, $[V(eba)_3]^{2-}$, $\Delta(V-C_{1,2}) = 0.003$ Å. This indicates that the catecholamide groups symmetrically span the coordination sphere in each of the complexes. The clearest comparison of the binding subunits in the two structures can be

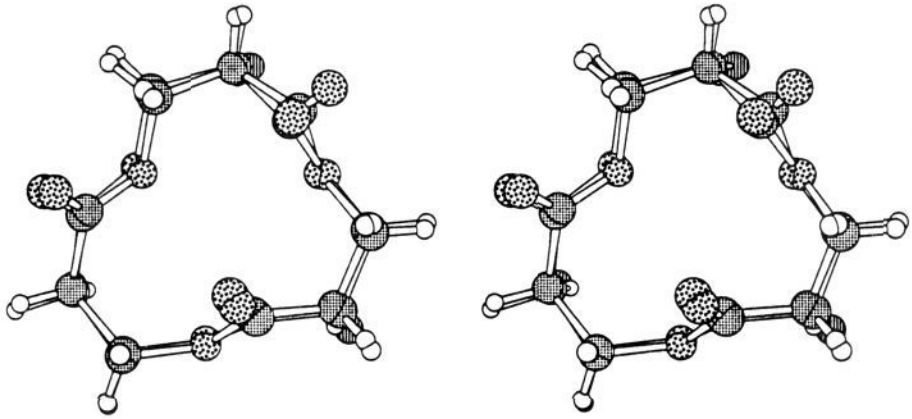

Figure 7. Stereoview of the backbone of $[V(ent)]^{2-}$ overlayed onto the Shanzer cyclic trilactone (ref 32).

seen by overlaying the subunits (Figure 6). Since the vanadium atom sits on a 3-fold axis in the crystal structure of $[V(eba)_3]^{2-}$, there is only one independent catecholamide group in the structure. In Figure 6 therefore, each of the three independent subunits in $[V(ent)]^{2-}$ are compared to the single subunit for $[V(eba)_3]^{2-}$, and the RMS error (for the nine atoms: V, O1, O2, C1 → C6) for each of the overlays is included. From each of the three comparisons in Figure 6 it is apparent that there is a slight difference in the relative position of the amide groups (clearest with the C comparison). This is also reflected in the dihedral angles between the amide group and the catechol (C_6) planes (Table I). There is thus a small perturbation in the structure of the catecholamide groups in $[V(ent)]^{2-}$ relative to $[V(eba)_3]^{2-}$, consistent with the smaller twist angle in the former.

Stereospecific Chelation in Metal–Enterobactin Complexes. The Δ chirality of $[Fe(ent)]^{3-}$ has a potential role in vivo. Since the mirror image Λ-ferric enantioenterobactin (which consists of *d*-serine units) is not effective in growth promotion as is the native Δ-$[Fe(ent)]^{3-}$ [45] and since it is known that the tris(catechol) portion of the molecule is essential for recognition by the *E. coli* outer membrane protein,[13] it has been suggested that it is the Δ chirality at the Fe center that is crucial in recognition of $[Fe(ent)]^{3-}$ (although recent results from this laboratory indicate that chiral discrimination does not occur at the outer membrane FepA protein).[46] It is thus desirable to understand the interactions that stabilize the Δ isomer in enterobactin–metal complexes. Shanzer et al. have proposed that the preference for the Δ conformation of $[Fe(ent)]^{3-}$ is a result of hydrogen bonding (between the amide protons and the ester oxygens of the serine backbone, O5 in Figure 2) that occurs in the free ligand prior to iron binding.[25] This analysis suggested that these bonds are broken once the ferric complex is formed. However, since Fe^{III} tris(catecholate) complexes are kinetically labile with respect to isomerization,[28] interactions which would stabilize the Δ isomer over the Λ isomer must be present in the metal–ligand complex. Furthermore, as will be shown in the next section of this paper, the structure of the enterobactin triserine ring precludes the hydrogen bonding proposed by Shanzer et al. It is our conclusion that the preference for the Δ isomer in metal–enterobactin complexes is a result of conformational constraints that exist *within* the 12-membered ring, and this can be seen in the structure of $[V(ent)]^{2-}$.

If a least-squares plane is defined by the 12-membered ring atoms of the enterobactin molecule, six atoms (C9A, B, C; C10A, B, C) sit above the plane and six sit below (O5A, B, C; C8A, B, C). At chiral C8, the bonds within the 12-membered ring (to C9 and C10) determine the tilt of the C8–N1 bond. Since each of the catecholamide arms remains planar (vide supra), the tilt of the C8–N1 bonds relative to the plane above sets the handedness of the propeller at the metal center. As a result of nonbonded interactions within the constraints of the 12-membered ring, C9 sits on average 0.27(4) Å higher above the plane than C10 (C9A, 0.282 Å; C9B, 0.296 Å; C9C, 0.232 Å) (Scheme I). This is turn causes the three bonds from C8 to N1 to tilt as a right-handed propeller (when viewed down the 3-fold axis) to maintain normal tetrahedral angles at C8.

The Fe^{III} complex of the enterobactin linear trimer, where the cyclic backbone is hydrolyzed at one position, has also been shown to preferentially form the Δ isomer with ≈80% of the optical activity of $[Fe(ent)]^{3-}$.[15] This observation is consistent with the fact that stabilizing interactions must be present in the metal–ligand complex to achieve stereoselectivity, since the H-bonding interactions suggested by Shanzer (which are ruled out by the backbone structure—see below) would not be expected in the linear trimer prior to iron binding.

The stabilization of the Δ isomer in $[V(ent)]^{2-}$ and the V^{IV} linear trimer complex has been further investigated using the MM2 molecular mechanics program on the CAChe system.[47] The geometry around the V^{IV} was locked to the geometry at the metal center found in the crystal structure of $[V(ent)]^{2-}$ (V–O distances fixed and the angles between the catechol oxygens fixed). Four minimizations were then performed: (1) Δ and (2) Λ metal center chirality with the enterobactin ligand and (3) Δ and (4) Λ metal center chirality with the linear trimer ligand. The Δ configuration of $[V(ent)]^{2-}$ was found to be stabilized by 29 kJ/mol over the Λ configuration, consistent with the CD spectrum of the ferric enterobactin complex in solution. The Δ configuration of the V^{IV} linear trimer complex was also found to be stabilized relative to Λ by 7.5 kJ/mol. This figure is consistent with the observed CD spectrum and a deduced ~80% retention of Δ chirality for the ferric linear trimer, since an energy difference of 6.0 kJ/mol would result in a 90% retention of configuration (and hence an 80% retention of optical activity).

The Enterobactin Backbone. The only difference in the enterobactin molecule and the model compounds MECAM and TRENCAM is the 12-membered ring backbone, and thus the backbone must play a key role in the observed stability of $[Fe(ent)]^{3-}$ relative to the model compounds. As can be seen in the side view of $[V(ent)]^{2-}$ (Figure 2), the 12-membered ring adopts a staggered conformation, similar to the chair conformation of cyclohexane. To determine if the backbone structure is perturbed upon metal binding, it can be compared to the structure of the cyclic trilactone itself, which has been reported by Shanzer and co-workers.[32] In Figure 7 is shown an overlay of the backbone in $[V(ent)]^{2-}$ and the cyclic trilactone. The structural similarities are remarkable, considering that in $[V(ent)]^{2-}$ there are three appended catecholamide groups bound to the metal center. The RMS error in overlaying the molecular fragments for the 12 ring atoms is 0.133 Å. That the backbone structure of enterobactin is not perturbed by the binding of the catecholamide groups to the vanadium center is another indication of the ideal size of the binding cavity of this molecule. The two crystal structures in

(45) Neilands, J. B.; Erickson, T. J.; Rastetter, W. H. *J. Biol. Chem.* **1981**, *256*, 3831.
(46) Nishio, T.; Bryan, B. L.; Raymond, K. N. Manuscript in preparation.
(47) Molecule Editor and Molecular Mechanics, Version 2.8; CAChe Scientific, Inc., 1991.

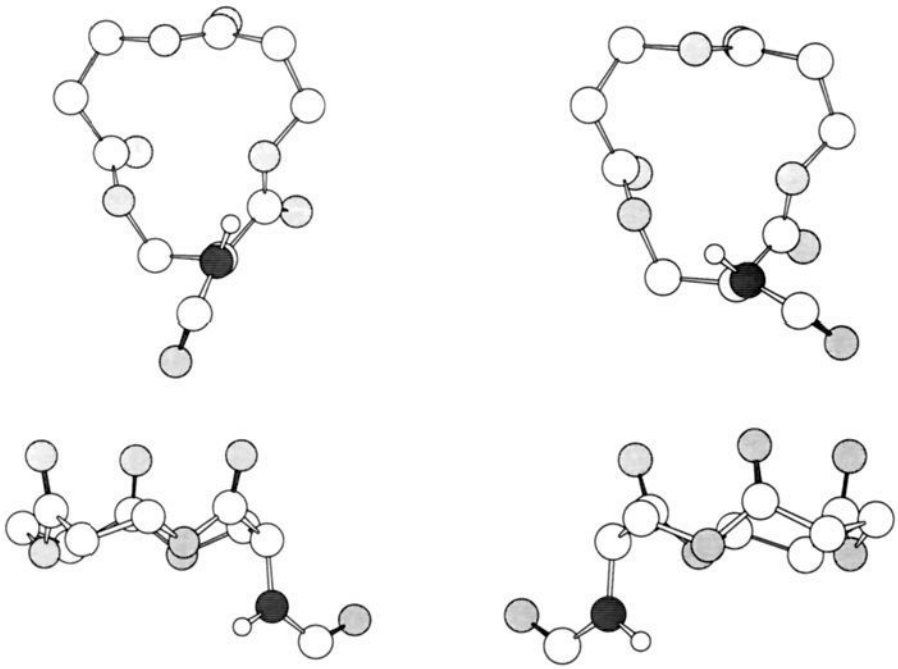

Figure 8. A computer graphics presentation of the closest approach for the amide N–H proton to the serine ester oxygens of enterobactin. Only one amide group is shown (average values for all three are given in the text). Top views are looking down on the ring. The bottom views are from the side. Left and right are the closest approach for clockwise and counterclockwise NH–O interactions, respectively.

Figure 7 show a conformation that is also very similar to that seen in another closely related cyclic trilactone structure.[48] The stability of this conformation for the triserine ring implies that this is also the conformation for the enterobactin ligand—which contradicts an earlier proposed structure.[24] Thus the catecholamide groups are in an *all-axial* orientation in both the free ligand and metal complexes of enterobactin; this conformation of the binding groups prior to metal binding accounts for much of the entropy portion of the higher thermodynamic stability of enterobactin relative to ligands which adopt splayed conformations—including TRENCAM, MECAM, and the enterobactin linear trimer.

The rigidity of the triserine ring fixes the orientation of the amide C–N bonds so that the only degree of freedom is rotation around this bond. The rotations which give the closest approach of the amide N–H proton to the ester oxygens are shown in Figure 8. These are the interactions that Shanzer et al. suggested as the origin for the Δ chirality of ferric enterobactin. However the average closest approach to the oxygen in the clockwise direction (left side of Figure 8) for the three different amides is 2.26 Å for the NH–O distance and the NHO angle is 103°. The corresponding parameters for the counterclockwise rotation (right side, Figure 8 —which would give a Λ metal ion configuration) are 2.58 and 98°, respectively. These are clearly not possible hydrogen bond interactions—and would also predict the wrong chirality.

Although the comparison cyclic trilactone structure is achiral, the same constraints should be operative that were discussed above as the source of stereospecificity in $[V(ent)]^{2-}$. If the same least-squares plane is defined for the trilactone structure, C9 is above C10 at two of the three carbons (by 0.208 and 0.324 Å), as is depicted in Scheme I. At the third carbon, C10 is above C9, however by only 0.085 Å. If catecholamide groups are then appended to the three C8 atoms in this structure, two binding groups will be predisposed to bind in a Δ fashion, whereas the third group will effectively show no preference. These results are thus in general agreement with the proposal that constraints within the backbone of enterobactin lead to stereospecific chelation.

Cation Coordination in the Structure of $K_2[V(ent)]\cdot 3DMF$. The coordination around K1 (six-coordinate) is a pseudo-trigonal prism

Scheme I

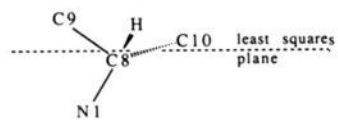

and K2 (five-coordinate) is a square pyramid. Both of the potassium ions are coordinated to the O2 atoms of the $[V(ent)]^{2-}$ anion, the carbonyl O3 atoms (see Figure 2 for anion labeling scheme) as well as to DMF oxygens (O1S, O2S, O3S). O3B and O3S bridge the two K^+ ions and the K–K distance is short (3.5 Å) relative to the average K–O distance of 2.6 Å. The basicities of the oxygens within the $[V(ent)]^{2-}$ anion explain the observed potassium coordination. The catecholate oxygens (O1 and O2) are the most basic; however, the O1 atoms are not very accessible (see Figure 2) because of the amide H-bonding. The O2 oxygens in the complex anion are therefore the most likely to be bound to Lewis acids in the solid state. Indeed, in each of the three other triscatecholamide structures characterized ($K_3[V(TRENCAM)]$,[41] $K_3[Fe(TRENCAM)]$,[28] and $K_2[V(eba)_3]$[42] similar K^+ coordination is seen. The amide carbonyl oxygens (O3) are the next most basic because of the delocalization of the double bond and thus are also bound to K^+ ions. There are no significant intermolecular interactions between the ester carbonyl atoms of the triserine ring (O4) and other atoms in the structure.

The interactions between the K^+ ions and the $[V(ent)]^{2-}$ anion are of interest because of an earlier study[49] which investigated the binding of Ca^{2+} to the ferric enterobactin complex. Hider et al. found that in 95% methanol the enterobactin complex has a considerable affinity for Ca^{2+} (association constant = 4×10^4 M^{-1}). In contrast, the ferric MECAM complex had no detectable affinity for Ca^{2+}. The authors concluded that the likely site for coordination of the calcium ion to the complex anion is in the cavity between the metal center and the backbone such that the Ca^{2+} ion is coordinated to six oxygens. This would explain the difference in affinity as seen for the MECAM complex, in which the cavity would be too small to allow incorporation of calcium.

Since K^+ is significantly larger than Ca^{2+} (K^+ = 1.38 Å; Ca^{2+} = 1.00 Å),[39] it was not expected that the structure of $K_2[V(ent)]$

(48) Seebach, D.; Müller, H.-M.; Bürger, H. M.; Plattner, D. A. *Angew. Chem., Int. Ed. Engl.* **1992**, *31*, 434.

(49) Hider, R. C.; Mohd-Nor, A. R.; Silver, J.; Neilands, J. B. *J. Inorg. Chem.* **1982**, *17*, 205.

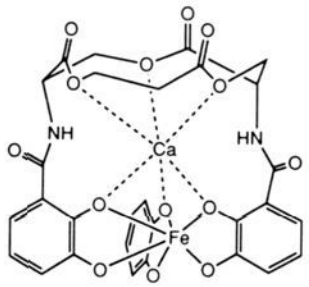

would demonstrate the "cavity-coordination" of one of the K^+ ions. However the possibility of calcium fitting into the cavity of the $[V(ent)]^{2-}$ anion was investigated using molecular visualization software.[47] A Ca^{2+} cation can be situated in the cavity of $[V(ent)]^{2-}$ to achieve six favorable 2.5 Å bonds to the oxygens; however, the amide protons congest the cavity since they are H-bonding to the O1 oxygens. For Ca^{2+} to reside within the cavity, the amide groups would have to rotate out of the way, which causes considerable strain in the molecule. Based on this and the Lewis basicity of the O2 oxygens, we believe that the more likely position for coordination of Ca^{2+} to $[Fe(ent)]^{3-}$ is to the O2 oxygens. However, since the binding of Ca^{2+} at this position is also available in the MECAM complex, we cannot explain the results of the earlier study.[49]

Absorption Spectra of $[V(ent)]^{2-}$. The UV/vis and circular dichroism (CD) spectra of $[V(ent)]^{2-}$ in water are shown in Figure 9. The UV/vis spectrum is almost identical to the spectra of $[V(TRENCAM)]^{2-}$[41] and $[V(eba)_3]^{2-}$[42] where the three bands between 400 and 800 nm are assigned to ligand-to-metal charge-transfer (LMCT) transitions and the band at 330 nm to a ligand $\pi-\pi^*$ transition. The CD spectrum in Figure 9 contains intense bands which correspond closely in energy to the bands seen in the UV/vis spectrum; however, there is an additional shoulder in the CD spectrum at ≈380 nm, for a total of four LMCT bands.

The LMCT bands in Fe^{III} tris(catecholates) have been definitively assigned using magnetic circular dichroism and single-crystal polarized absorption spectroscopies.[23] Can those results be used to assign the bands in $[V(ent)]^{2-}$ (and in other V^{IV} tris(catecholates))? The transitions in the CD spectrum of $[V(ent)]^{2-}$ were modeled with a Gaussian fitting program,[50] and the transition energies are presented in Table II with the proposed band assignments (there is an additional CD band (262 nm) in Table II which is not shown in Figure 9). In Figure 10 is shown the molecular orbital scheme which depicts the LMCT transitions as assigned for $[V(ent)]^{2-}$. The analysis is performed in D_3 symmetry—the ligand HOMOs a_2 and e_π are derived from the three $p\pi$ catecholate MOs with the phasing shown on the right of Figure 10.[23] Transitions I–IV were the four lowest energy LMCT transitions observed in the Fe^{III} tris(catecholates) and are thus assigned as the four lowest energy bands in $[V(ent)]^{2-}$. As outlined for the iron complexes,[23] the parameter γ (Figure 10) indicates the amount of π bonding and can be calculated by the energy difference between transitions I and II or III and IV. That both methods of calculating γ result in essential the same value for $[V(ent)]^{2-}$ (II–I = 3898 cm^{-1}; IV–III = 4025 cm^{-1}) is evidence for these assignments being correct. Further evidence is given by the sign of the CD transitions in $[V(ent)]^{2-}$ compared to the CD transitions in $[Fe(ent)]^{3-}$.[38,51] In $[Fe(ent)]^{3-}$, only LMCT transitions I and II can be observed in the CD spectrum; however, these are the same sign (I, negative; II, positive) as the transitions assigned to I and II in the spectrum of $[V(ent)]^{2-}$. Hence the assignments of the LMCT transitions as determined for the Fe^{III} tris(catecholates) are also applicable to the V^{IV} tris(catecholates).

Having determined the assignments for the bands in the spectra of $[V(ent)]^{2-}$, the bonding parameters γ and μ (Figure 10) can be determined as was done for the Fe^{III} tris(catecholates). The parameter, γ, which is a measure of π bonding, is calculated to be 3898 cm^{-1},[52] and μ, which is a measure of σ bonding, is calculated to be 8419 cm^{-1}. Ideally, these values should be compared to $[Fe(ent)]^{3-}$; however, in our previous investigation[23] we obtained

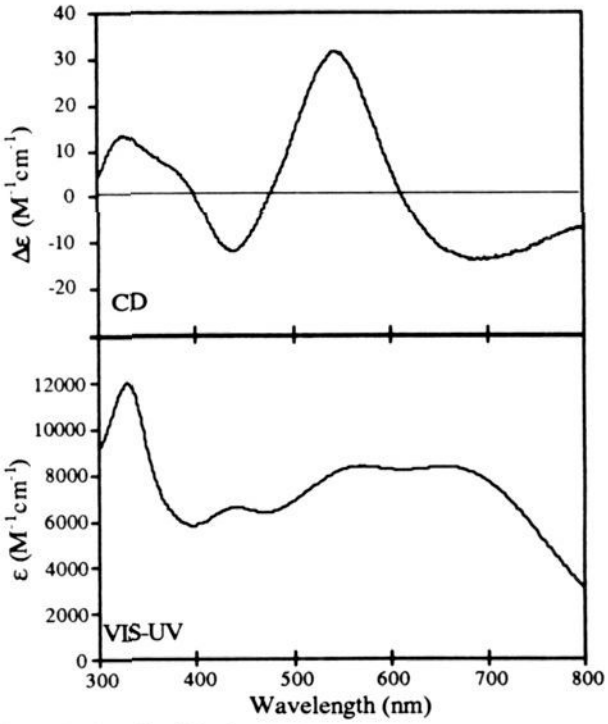

Figure 9. Circular dichroism (top) and UV/vis (bottom) spectra of $[V(ent)]^{2-}$ (H_2O, pH 7).

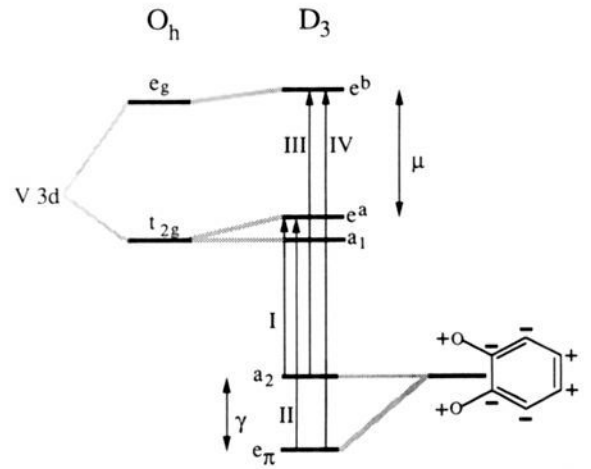

Figure 10. One-electron molecular orbital energy level diagram for $[V(ent)]^{2-}$. The observed LMCT transitions (labeled with Roman numerals) originate at the catecholate HOMOs a_2 and e_π and terminate at the metal d-orbitals.

Table II. Assignments and Transition Energies for the Circular Dichroism Spectrum of $[V(ent)]^{2-}$ (H_2O, pH 7)

band[a]	assignment	energy (cm^{-1})	wavelength (nm)	$\Delta\epsilon$ (M^{-1} cm^{-1})
I	LMCT: $a_2 \rightarrow e^a$	14479	691	−13.9
II	LMCT: $e_\pi \rightarrow e^a$	18377	544	+31.7
III	LMCT: $a_2 \rightarrow e^b$	22898	437	−11.9
IV	LMCT: $e_\pi \rightarrow e^b$	26923	371	≈+7
	ligand $\pi-\pi^*$	30570	327	+13.6
	ligand $\pi-\pi^*$	38098	262	−20.5

[a] See Figure 10.

(50) Gebhard, M. S.; Deaton, J. C.; Koch, S. A.; Millar, M.; Solomon, E. I. *J. Am. Chem. Soc.* **1990**, *112*, 2217.
(51) Salama, S.; Stong, J. D.; Neilands, J. B.; Spiro, T. G. *Biochemistry* **1978**, *17*, 3781.

Table III. Summary of Crystallographic Data and Parameters

	K_2[V(ent)]·3DMF	K_2[V(eba)$_3$]·3DMF
formula	$VK_2O_{18}N_6C_{39}H_{42}$	$VK_2O_{12}N_6C_{36}H_{48}$
formula wt	1011.95	885.96
temp (K)	172	168
crystal system	monoclinic	cubic
space group	$P2_1$ (no. 4)	$Pa\bar{3}$ (no. 205)
a (Å)	13.164 (3)	20.632 (5)
b (Å)	10.001 (1)	
c (Å)	16.600 (2)	
β (deg)	93.96 (1)	
Z	2	8
V (Å^3)	2180 (1)	8783 (5)
μ_{calc} (cm^{-1})	4.90	4.67
δ_{calc} (g·cm^{-1})	1.541	1.340
F(000)	1046	3704
crystal size (mm)	0.08 × 0.45 × 0.50	0.31 × 0.46 × 0.49
radiation	Mo Kα (λ = 0.71073 Å)	Mo Kα (λ = 0.71073 Å)
h,k,l range collected	0 → 14, 0 → 10, ±17 and	0 → 24, 0 → 24, 0 → 24
	0 → −14, 0 → −10, ±17	($l > h$, $l > k$)
2θ range	3.0–45.0°	3.0–50.0°
scan type	θ–2θ	θ–2θ
scan speed (°/min)	4.1	5.6
reflcns collected	6377	2946
unique reflcns	6348	2576
data: $F_o^2 > 3\sigma(F_o^2)$	5551	1247
no. of parameters	600	199
data/parameter ratio	9.3	6.3
R	0.049	0.051
R_w	0.062	0.058
goodness of fit	1.81	1.44

the parameters for the complex [Fe(TRENCAM)]$^{3-}$, which has identical spectral features to [Fe(ent)]$^{3-}$. For [Fe(TRENCAM)]$^{3-}$, γ = 3495 cm^{-1} and μ = 7193 cm^{-1}. The increase in both of these bonding parameters for [V(ent)]$^{2-}$ relative to [Fe(TRENCAM)]$^{3-}$ indicates that the M–O bonding is stronger in [V(ent)]$^{2-}$—a consequence of the higher charge on the metal cation.

The observed spectroscopic differences between [Fe(TRENCAM)]$^{3-}$, [Fe(ent)]$^{3-}$ and [V(ent)]$^{2-}$ can be further analyzed to approximate the energy of the d-orbitals of V^{IV} relative to Fe^{III} (Figure 11). Since all the LMCT transitions of [V(ent)]$^{2-}$ are lower in energy than in [Fe(TRENCAM)]$^{3-}$, it follows that the d-orbitals are at lower energy in the vanadium(IV) complex. The ligand a_2 orbital (Figures 10 and 11) is virtually nonbonding and therefore provides a reference point for the molecular orbitals. The energy difference between transitions I in [V(ent)]$^{2-}$ and [Fe(TRENCAM)]$^{3-}$ (I_{Fe}–I_V in Figure 11) is 4300 cm^{-1}. Since the metal e^a orbital will be destabilized more in the V^{IV} complexes than in the Fe^{III} complexes, the value of (I_{Fe}–I_V) is not equal to the energy difference between the metal d orbitals (Δd in Figure 11). The *difference* in the amount of e^a destabilization between the V^{IV} and Fe^{III} complexes will however be approximately the same as the *difference* in the e_π stabilization between the complexes. The difference in the latter stabilization is reflected in the different γ values for the metal complexes. The value for γ in [V(ent)]$^{2-}$ is 400 cm^{-1} greater than in [Fe(TRENCAM)]$^{3-}$, allowing an estimate for Δd to be made as 4700 cm^{-1} (I_{Fe}–I_V + $\Delta\gamma$).

Electrochemistry. The electrochemistry of the complexes [V(ent)]$^{2-}$, [V(eba)$_3$]$^{2-}$, and [V(TRENCAM)]$^{2-}$ was investigated in DMF, and the resultant cyclic voltammograms are shown in Figure 12. All three complexes show essentially reversible waves (peak separations of 64 mV with a ratio of cathodic to anodic peak currents near unity). These waves are assigned as the V^V/V^{IV} couple since the V^{IV}/V^{III} couple would be expected at ≈−0.7 V vs SCE.[36,41] The redox potentials are +0.39 V for [V(ent)]$^{2-}$,

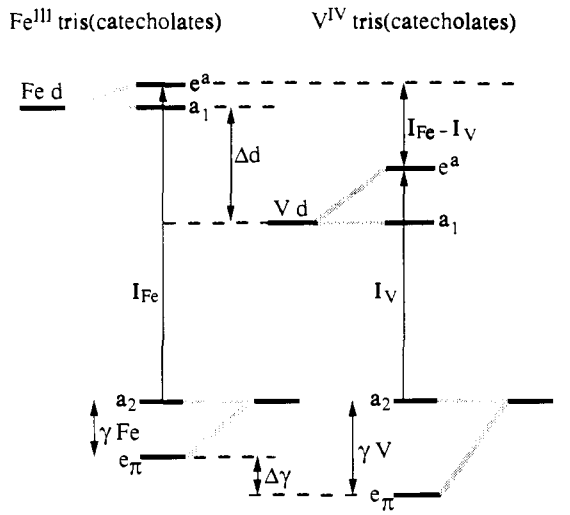

Figure 11. Relative molecular orbital energy level diagrams for Fe^{III} tris(catecholates) and V^{IV} tris(catecholates).

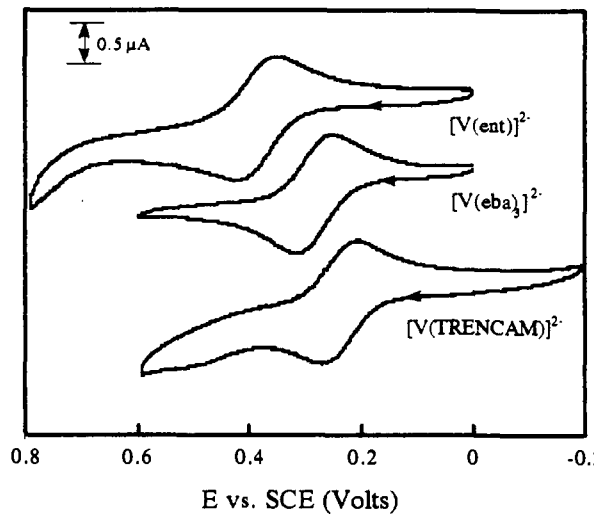

Figure 12. Cyclic voltammograms of the three vanadium complexes in DMF vs SCE. Conditions: ca. 1.0 mM metal complex concentration, 0.1 M Bu_4NPF_6, Pt disk working electrode, scan rate 75 mV/s.

+0.28 V for [V(eba)$_3$]$^{2-}$, and +0.24 V for [V(TRENCAM)]$^{2-}$ vs SCE. The V^{IV} ion is thus stabilized more effectively in [V(ent)]$^{2-}$, which is also manifest in the reduced oxygen sensitivity of [V(ent)]$^{2-}$ relative to the other two complexes. Because the binding groups are not constrained in [V(eba)$_3$]$^{2-}$, the catecholate ligands can reorient more easily to stabilize the smaller V^V ion. The fact that TRENCAM stabilizes V^V better than enterobactin is consistent with the structural analyses which indicate that the cap in TRENCAM is too small for effective coordination of Fe^{III} and V^{III}, however, appears better suited for the smaller V^V ion (0.54 Å).[39]

Conclusions

The siderophore enterobactin is produced in microbes for effective chelation and transport of Fe^{III}. The features that lead to the remarkable stability of the ferric enterobactin complex are revealed by the crystal structure of the vanadium(IV) complex, [V(ent)]$^{2-}$. The size of the enterobactin backbone appears to play a substantial role in the observed stability of [Fe(ent)]$^{3-}$, since it provides the optimum spacing between the three binding subunits. The conformation of the backbone is also a key to the stability of [Fe(ent)]$^{3-}$. In addition, the stereospecific chelation in enterobactin complexes can be ascribed to constraints within the backbone. Finally, it has been determined through analysis of the LMCT transitions in [V(ent)]$^{2-}$ that the σ and π metal–oxygen bonding is stronger than in [Fe(ent)]$^{3-}$.

Experimental Section

Physical Measurements. Absorption spectra were recorded on a Hewlett-Packard 8450A UV/vis diode array spectrophotometer. Circular dichroism spectra were collected on a Jasco J-500C spectropolarimeter equipped with an IF-500 II A/D converter. Crystal data were collected on an Enraf-Nonius CAD-4 diffractometer. Cyclic voltammograms were collected using a BAS 100A electrochemical analyzer. All potentials were measured anaerobically and are relative to the saturated calomel electrode (SCE) (uncorrected for junction potentials). Distilled, anhydrous DMF solutions were 0.1 M in Bu_4NPF_6. The Fc^+/Fc couple was measured in DMF using identical conditions and found to be +0.480(5) V (vs SCE). FAB mass spectra were performed by the Mass Spectrometry Laboratory, College of Chemistry, University of California, Berkeley. Microanalyses were performed by the Analytical Services Laboratory, College of Chemistry, University of California, Berkeley. Analyses that were within 0.4% of the calculated values were considered acceptable.

Preparation of Compounds. All manipulations were performed using standard Schlenk techniques under Ar. H_6(enterobactin)·H_2O was isolated from cultures of *E. coli* AN311 as previously described.[53] H_6(TRENCAM)·HBr was synthesized according to the literature method.[19] Vanadyl bis(acetylacetonate), $VO(acac)_2$, was recrystallized before use ($CHCl_3$/acetone).

K_2[V(ent)]·3DMF. To 25 mg of $H_6(ent)·H_2O$ (0.036 mmol) in degassed MeOH was added 9.5 mg of $VO(acac)_2$ (0.036 mmol). A solution of KOH in degassed MeOH (0.072 mmol) was added via cannula resulting in a deep blue solution which was taken to dryness yielding a blue-black solid, K_2[V(ent)], which is air-stable in the solid state indefinitely. The complex will only decompose in aqueous solution (pH 7) if exposed to oxygen for several weeks. Crystals of K_2[V(ent)·3DMF were grown via vapor diffusion of Et_2O into a DMF solution of K_2[V(ent)]. Elemental Anal. for $K_2VC_{30}H_{21}N_3O_{15}$·3DMF: C, H, N. MS (−FAB) *m/e* 715 ([V(ent)]H^-).

K_2[V(TRENCAM)]. The synthesis of the ammonium salt has been previously reported.[41] To 150 mg H_6TRENCAM·HBr (0.236 mmol) in degassed MeOH was added a solution of KOH (0.68 mmol, 2.9 equiv) in MeOH. $VO(acac)_2$ (62.6 mg, 0.24 mmol) was then added, and the solution immediately turned very dark blue. The solution was stirred at room temperature for 1 h and then taken to dryness. The solid was dissolved in a minimum of MeOH and applied to a Sephadex LH-20 column (MeOH). The complex eluted as a single band, was collected, and taken to dryness. The blue/black solid was stored under Ar. Solutions of the complex will decompose if exposed to oxygen for periods of hours. Elemental Anal. for $VK_2C_{27}H_{24}N_4O_9$: C, H, N.

H_2(eba). 2,3-Dimethoxybenzoic acid (8.01 g, 44.0 mmol) was dissolved in 250 mL of CH_2Cl_2 and the solution stirred vigorously. Dicyclohexylcarbodiimide (9.72 g, 47.1 mmol) was then added followed by the addition of 2-mercaptothiazoline (5.27 g, 44.0 mmol) and catalytic 4-(dimethylamino)pyridine (DMAP) (100 mg). The mixture was stirred for 24 h, and the white precipitate of *N,N'*-dicyclohexylurea filtered from the yellow solution, which was evaporated to a yellow oil. Excess 2-mercaptothiazoline was removed from the oil by successive extraction of a CH_2Cl_2 solution of the oil with 3 × 100 mL of 0.1 M NaOH. After drying the organic phase over $MgSO_4$ and evaporation under reduced pressure, the yellow solid was recrystallized from $CHCl_3$/hexanes to give 9.97 g (80%) of yellow crystals of 3-(2,3-dimethoxybenzoyl)-1,3-thiazolidine-2-thione: mp 123–124.5 °C; ^{1}H NMR ($CDCl_3$) δ 7.07 (t, 1 H, *J* = 7.9 Hz), 7.00 (dd, 1 H, J_1 = 8.2 Hz, J_2 = 1.5 Hz), 6.90 (dd, 1 H, J_1 = 7.7 Hz, J_2 = 1.5 Hz), 4.63 (t, 2 H, *J* = 7.3 Hz), 3.92 (s, 3 H), 3.87 (s, 3 H), 3.41 (t, 2 H, *J* = 7.3 Hz). Elemental Anal. for $C_{12}H_{13}NO_3S_2$: C, H, N, S.

Ethylamine (2.00 g, 31.0 mmol) as a 70% aqueous solution was dissolved in 300 mL of 0.1 M NaOH and 3-(2,3-dimethoxybenzoyl)-1,3-thiazolidine-2-thione (7.00 g, 25.0 mmol) was dissolved in 250 mL of $CHCl_3$, and the two phases stirred vigorously overnight, during which time the organic layer became colorless. The $CHCl_3$ phase was separated and extracted with 2 × 200 mL of 0.2 M HCl, 2 × 200 mL of 0.1 M NaOH, and 200 mL of brine and then dried over $MgSO_4$. Removal of the solvents afforded a slightly yellow oil, Me_2(eba) (5.15 g, 98% crude yield), which was demethylated without further purification.

The methyl-protected ligand was dissolved in 200 mL of dry CH_2Cl_2, and the solution deoxygenated. Neat BBr_3 (18.90 mL, 0.200 mol) was added to the vigorously stirred solution via syringe, resulting in the formation of a tan precipitate. The flask was equipped with a drying tube and stirred for 2 days, and the reaction mixture quenched with H_2O (1000 mL). The H_2O/CH_2Cl_2 mixture was brought to a boil, and the volume was reduced to ca. 900 mL and then allowed to cool to room temperature. The aqueous layer was extracted with 4 × 300 mL of $CHCl_3$, and the organic extracts evaporated to a brown oil. The crude oil was flash-chromatographed on a silica gel column and eluted with 1% HOAc/3% MeOH/CH_2Cl_2. The slightly brown oil thus obtained was recrystallized from CH_2Cl_2/hexanes to afford the product as colorless blocks (4.19 g, 92%): ^{1}H NMR ($CDCl_3$) δ 12.79 (s, 1 H), 7.04 (dd, 1 H, J_1 = 6.7 Hz, J_2 = 1.2 Hz), 6.88 (dd, 1 H, J_1 = 6.9 Hz, J_2 = 1.2 Hz), 6.74 (t, 1 H, *J* = 8.0 Hz), 6.38 (unres. t, 1 H), 5.91 (s, 1 H), 3.49 (m, 2 H), 1.26 (t, 3 H, *J* = 7.3 Hz). Elemental Anal. for $C_9H_{11}NO_3$: C, H, N.

K_2[V(eba)$_3$]·3DMF. A solution of 2.06 mL of 0.5 M KOH/EtOH (1.03 mmol) and H_2(eba) (0.280 g, 1.55 mmol) in 25 mL of EtOH was transferred via cannula into a solution of $VO(acac)_2$ (0.137 g, 0.52 mmol) in 25 mL of EtOH, resulting in the immediate formation of a deep blue solution. This solution was stirred for 2 h at room temperature, and the ethanol was removed to give a deep blue solid, which was recrystallized from DMF/Et_2O to give cubic crystals. Elemental Anal. for $C_{27}H_{27}N_3O_9VK_2$·3DMF: C, H, N.

Crystallography. General Methods. Crystals were mounted on glass fibers in Paratone N oil, transferred to an Enraf-Nonius CAD-4 automated four-circle diffractometer, and then cooled (<195 K) under a stream of nitrogen. After visual centering of the crystal in the beam, primitive cell constants were determined by least-squares treatment of 24 strong, high-angle ($\theta \approx 12°$) reflections well-spaced throughout reciprocal space. Automated indexing procedures were employed to determine the crystal system and give a preliminary space group assignment. Data were collected using the θ-2θ scan technique. Three orientation and intensity control reflections were monitored every 200 reflections and every hour of data collection, respectively. Azimuthal (ψ) scans were recorded for three or four strong reflections with $\chi > 80°$ at the end of each data collection. Crystal data and data collection parameters are summarized in Table III.[42]

After reduction of the data and correction for Lorentz and polarization effects, the intensity check reflections were examined for evidence of crystal decay over the period of data collection. Empirical absorption corrections were applied to each of the data sets on the basis of the ψ scan data. The structures were solved using the direct methods program SHELXS-86. Hydrogen atoms for both structures were included in the final cycles of refinement at calculated positions 0.95 Å from, and with B_{iso} 1.25 times that of, the parent atom.

K_2[V(ent)]·3DMF. X-ray quality crystals were grown from a DMF solution of the complex by vapor diffusion of Et_2O at room temperature over 6 weeks. Data collection and crystal parameters for the structure are provided in Table III. The data were collected in two sets: $(h,k,\pm l)$ and Friedel pairs $(-h, -k, \pm l)$ from $3° \leq 2\theta \leq 45°$. A three-segment linear decay correction was applied to the data after inspection of the intensity standards. The unit cell parameters indicated a monoclinic space group with $Z = 2$. Systematic extinctions were indicative of a 2_1 screw-axis parallel to b, and thus the space group $P2_1$ was chosen. The chirality of the ligand supported this noncentrosymmetric space group. The *y*-coordinate of the vanadium atom was set at 0.124 to fix the origin in this polar space group.

Three atoms in the DMF molecules were found to be disordered: O1S over two positions, and the occupancy was set at 0.65/0.35; C1S over three positions, 0.50/0.25/0.25; C7S over three positions, 0.50/0.25/0.25. All non-hydrogen atoms in the structure (except those with partial occupancy) were refined anisotropically. All hydrogen atoms in the [V(enterobactin)]$^{2-}$ anion were included at calculated positions for structure factor calculations but were not refined. Full matrix least-squares refinement yielded $R = 0.049$ and $R_w = 0.062$ for 600 parameters and 5551 reflections with $I \geq 3\sigma(I)$. Positional parameters are listed in Table IV.[42]

The chirality of the three C8 atoms derived from *l*-serine (*S,S,S*) defines the correct enantiomorph in the crystal structure solution. The trischelate isomer could then be assigned as Δ. Nonetheless, the enantiomeric Λ (*R,R,R*) structure was also refined as an internal check and yielded $R = 0.054$ and $R_w = 0.067$.

K_2[V(eba)$_3$]·3DMF. Crystals suitable for diffraction were grown by diffusion of ether into a DMF solution. After centering, automated indexing procedures indicated primitive cubic symmetry, and inspection of a small shell ($3° \leq 2\theta \leq 10°$) of data revealed *m*3 Laue symmetry (*not* *m*3*m*), with $Z = 8$ (4Δ and 4Λ). A unique set of data was collected (h, k, l range $0 \rightarrow 24$; $l > h$ and $l > k$). Data collection and crystal parameters for the structure are provided in Table III. Inspection of the intensity standards indicated no crystal decomposition during the data collection. The structure was solved using SHELXS, which revealed the vanadium and the two potassiums sitting on a 3-fold axis and some of the unique eba ligand, as well as some solvent structure. Least-squares refinement on just the vanadium and potassiums revealed the entire

(52) The difference between transitions I and II was used for the calculation of γ since the Gaussian fitting of the shoulder (band IV) at 370 nm is less accurate than the fitting of I and II.

(53) Young, I. G.; Gibson, F. *Methods Enzymol.* **1979**, *56*, 394.

unique ligand and the solvent DMF. Subsequent iterations of least squares cycles and difference Fourier calculations revealed solvent disorder. The solvent disorder was successfully modeled with 0.57/0.43 occupancies for all except the O4 of the solvent DMF. In the latter cycles of refinement, hydrogen atoms were included at calculated positions for structure factor calculations but were not refined. Full matrix least-squares refinement yielded $R = 0.051$ and $R_w = 0.058$ for 199 parameters and 1247 reflections with $I \geq 3\sigma(I)$. Positional parameters are listed in Table V.[42]

Acknowledgment. This research was funded by the National Institutes of Health Grant AI 11744. The authors also wish to acknowledge Mr. Ryan Powers for performing the MM2 calculations on the Δ and Λ vanadium complexes of the linear trimer and enterobactin.

Supplementary Material Available: Tables of bond lengths, bond angles, torsional angles, anisotropic thermal parameters, and positional parameters for the two structures $K_2[V(ent)]\cdot 3DMF$ and $K_2[V(eba)_3]\cdot 3DMF$, ORTEP views of the potassium coordination in both structures, and the UV/vis spectrum of the complex $[V(eba)_3]^{2-}$ (18 pages). Ordering information is given on any current masthead page.

Dioxygen Binding to Diferrous Centers. Models for Diiron-Oxo Proteins†

Yanhong Dong, Stéphane Ménage, Bridget A. Brennan, Timothy E. Elgren, Ho G. Jang, Linda L. Pearce, and Lawrence Que, Jr.*

Contribution from the Department of Chemistry, University of Minnesota, Minneapolis, Minnesota 55455. *Received August 24, 1992*

Abstract: Dioxygen adducts of $[Fe_2L(O_2CC_6H_5)]X_2$, where L represents the dinucleating ligands HPTB (anion of *N,N,N',N'*-tetrakis(2-benzimidazolylmethyl)-2-hydroxy-1,3-diaminopropane), its *N*-ethyl analogue, and its tetrakis(pyridine) analogue, HPTP, can form and serve as models for the putative oxygenated intermediates of methane monooxygenase and ribonucleotide reductase. $[Fe_2(N\text{-Et-HPTB})(O_2CC_6H_5)](BF_4)_2$ (**1**) crystallizes in the triclinic space group $P\bar{1}$ with cell constants $a = 13.04$ (1) Å, $b = 14.248$ (7) Å, $c = 18.09$ (1) Å, $\alpha = 73.56$ (6)°, $\beta = 78.22$ (7)°, $\gamma = 67.71$ (6)°, $V = 2963$ (9) Å^3, $Z = 2$; $R = 0.069$, and $R_w = 0.085$. The Fe(II) sites are bridged by the alkoxide of the dinucleating ligand and a benzoate, affording a diiron core with an Fe-μ-O-Fe angle of 124.0 (3)° and an Fe-Fe distance of 3.473 (7) Å. Both Fe(II) centers have trigonal bypyramidal geometry, and NMR studies show that the remaining coordination sites are accessible to ligands such as DMSO and Ph_3PO. The iron centers are antiferromagnetically coupled with $J \sim 20$-26 cm^{-1} ($\mathcal{H} = JS_1\cdot S_2$). Irreversible dioxygen adducts form upon exposure of the diferrous complexes to O_2 at low temperatures. The $\mathbf{1}/O_2$ adduct and its HPTB analogue, $\mathbf{2}/O_2$, are stable indefinitely in CH_2Cl_2 at −60 °C but decompose upon warming; the addition of DMSO or other polar aprotic solvents further stabilizes the adducts, allowing them to persist for short periods even at ambient temperature. The adduct of the pyridine analogue, $\mathbf{3}/O_2$, on the other hand, is not observed at −80 °C unless a polar aprotic solvent is added to the CH_2Cl_2 solution. The adducts exhibit visible absorption maxima near 600 nm and resonance Raman features at ~470 cm^{-1} (ν(Fe-O)) and ~890-900 cm^{-1} (ν(O-O)). The latter is characteristic of a μ-1,2-peroxo species; in support, the NMR properties of the HPTB adducts indicate the presence of a moderately strong antiferromagnetic coupling interaction ($J \sim 140$ cm^{-1}). Carboxylate substitution on **1** effects a shift of the absorption maximum of the adduct, indicating that the carboxylate remains coordinated in the adduct. Thus, the adducts are proposed to have tribridged (μ-1,2-peroxo)(μ-carboxylato)(μ-alkoxo)diferric cores. The differing stabilities of the dioxygen adducts are also reflected in differences in reactivity. The addition of 2,4-di-*tert*-butylphenol or Ph_3P does not affect the $\mathbf{1}/O_2$ adduct at −50 °C but does accelerate the decomposition of the $\mathbf{3}/O_2$ adduct, affording 0.5-0.6 equiv of the corresponding biphenol or $OPPh_3$, respectively. The one-electron oxidation of a phenol by $\mathbf{3}/O_2$ suggests that such an oxygenated species may be involved in the mechanism of the tyrosyl radical formation in ribonucleotide reductase; however, some further activation step is likely to be required for such a species to participate in the alkane hydroxylation mechanism of methane monooxygenase.

Introduction

Diiron centers that are known to interact with dioxygen[1] have been found in hemerythrin (Hr),[2,3] ribonucleotide reductase (RNR),[4-7] and methane monooxygenase (MMO).[8,9] DeoxyHr reversibly binds dioxygen to form oxyHr, characterized as a (μ-oxo)diiron(III) complex with a terminally bound hydroperoxide.[3] The adduct exhibits a purple color ($\lambda_{max} = 500$ nm) ascribed to a peroxide-to-iron(III) charge-transfer band.[10] The diferrous form of the R2 protein of ribonucleotide reductase also reacts with dioxygen to form a colored intermediate ($\lambda_{max} = 565$ nm) proposed to be a dioxygen adduct of the diiron active site which decays to the active protein containing the catalytically essential tyrosine radical.[11] The diferrous form of the hydroxylase of methane monooxygenase (MMO) has been demonstrated to react with dioxygen,[9a] but no intermediate has been observed; additionally, its diferric form reacts with H_2O_2 to oxidize alkanes in a peroxide shunt mechanism analogous to that observed for cytochrome

† Dedicated to Professor Richard H. Holm in celebration of his 60th birthday.

(1) Que, L., Jr.; True, A. E. *Prog. Inorg. Chem.* **1990**, *38*, 97-200.
(2) (a) Wilkins, P. C.; Wilkins, R. G. *Coord. Chem. Rev.* **1987**, *79*, 195-214. (b) Klotz, I. M.; Kurtz, D. M., Jr. *Acc. Chem. Res.* **1984**, *17*, 16-22.
(3) (a) Holmes, M. A.; Trong, I. L.; Turley, S.; Sieker, L. C.; Stenkamp, R. E. *J. Mol. Biol.* **1991**, *218*, 583-593. (b) Sheriff, S.; Hendrickson, W. A.; Smith, J. L. *J. Mol. Biol.* **1987**, *197*, 273-296. (c) Stenkamp, R. E.; Sieker, L. C.; Jensen, L. H.; McCallum, J. D.; Sanders-Loehr, J. *Proc. Natl. Acad. Sci. U.S.A.* **1985**, *82*, 713-716.
(4) Reichard, P.; Ehrenberg, A. *Science (Washington, D.C.)* **1983**, *221*, 514-519.
(5) Nordlund, P.; Sjöberg, B.-M.; Eklund, H. *Nature* **1990**, *345*, 593-598.
(6) Lynch, J. B.; Juarez-Garcia, C.; Münck, E.; Que, L., Jr. *J. Biol. Chem.* **1989**, *264*, 8091-8096.
(7) Sahlin, M.; Gräslund, A.; Petersson, L.; Ehrenberg, A.; Sjöberg, B.-M. *Biochemistry* **1989**, *28*, 2618-2625.
(8) DeWitt, J. G.; Bentsen, J. G.; Rosenzweig, A. C.; Hedman, B.; Green, J.; Pilkington, S.; Papaefthymiou, G. C.; Dalton, H.; Hodgson, K. O.; Lippard, S. J. *J. Am. Chem. Soc.* **1991**, *113*, 9219-9235.

0002-7863/93/1515-1851$04.00/0